Resonance and Continuum Components of the Strength Function *)

Takayuki Myo, Akira Ohnishi and Kiyoshi Katō

Division of Physics, Graduate School of Science, Hokkaido University, Sapporo 060

(Received July 26, 2002)

It is shown that the strength function can be expressed in a sum of the contributions from bound, resonance and continuum terms and the role of each term can be investigated complementarily by using the complex scaling method (CSM). The mechanism of the Coulomb breakup reaction of ^{11}Be is analyzed and we confirm the fact that the breakup is direct but not through resonances. The present method is also applied to other systems and its usefulness is discussed.

§1. Introduction

A new field of nuclear physics has been recently developed with the great advances of experimental techniques using unstable nuclear beams. Those experimental developments have provided us with findings of anomalous phenomena of unstable nuclei near the drip line. The most typical discovery is a neutron halo structure in several neutron-rich nuclei such as ^{11}Li,^{11}Be,^{14}Be and ^{17}B.[1] In these nuclei, a local breaking of the density and the binding-energy saturations which have been believed as the most basic properties of nuclei, has been shown.

One of the common features of unstable nuclei is the weak binding; the neutron halo nuclei have extremely small binding energies against the one- or two-neutron emissions, which indicate the necessity to take into account the effect from unbound states properly for the description of bound states. For example, the ground state of ^{11}Li has the binding energy of about 300 keV[1] from the ^{9}Li+n+n threshold, and its halo structure must receive much effect from unbound configurations. Inversely, the weak binding state or the halo structure is considered to give a strong influence on the property of unbound states. The soft-dipole giant resonance is one of the most interesting problems[2] concerning a characteristic excitation mode originated from the weak binding.

In order to investigate those properties of unstable nuclei, it is necessary to treat both bound and unbound states on the same footing. For nuclear many-body systems, many excellent methods have been developed to describe characteristic properties of bound and unbound states. However, they are applied to those states separately. We want to describe unbound states within the same many-body theory of bound states. For such an aim, the complex scaling method, abbreviated as CSM hereafter, seems very promising because unbound resonances can be described as square integrable states with the same boundary condition as that of bound states.[3] In CSM, therefore, resonance solutions can be obtained by using the same techniques

*) Published in Prog. Theor. Phys. **99** (1998), pp 801-817.

typeset using $\mathcal{PTP}$TEX.cls ⟨Ver.0.85⟩

developed for the bound-state problems of a many-body system.

The resonance energy and the decay width have been calculated in CSM[4)−10)] up to today in order to clarify the binding mechanism of several nuclei near the drip line. However in addition to them other physical quantities such as root-mean-square radii and transition probabilities are expected to play an important role in understanding the properties of resonances in detail, and for this purpose the extension of the applicability of CSM is necessary. In the first paper of our work,[11)] we discussed the definition, the calculational way and the meaning of matrix elements associated with resonances in CSM. We showed CSM to be also useful for calculating of these quantities, and discussed the interesting character of resonance states in the energy-weighted sum-rule value. For a schematic potential model, the contribution to the dipole transition strength from resonance states is shown to be very large and to exhaust most of the sum rule value.

In the second paper,[12)] we explicitly discussed the contribution to the transition strength not only from bound and resonance states but also from continuum ones, where continuum states are defined to be residual unbound states excluding resonances. Such a separation of unbound states into resonance and continuum ones is guaranteed by the extended completeness relation (ECR) which has been proposed and discussed by Berggren[13)] and Romo.[14)] We presented that CSM provides us with a natural way to separate resonance and continuum solutions satisfying ECR. In CSM, this separation depends on the scaling angle θ, and the number of resonances constructing ECR increases with θ. The calculated results about the sum rule values for several transition operators show that as the number of resonances constructing ECR increases, the contributions of the resonance states to the sum rule values increase, but on the contrary those from continuum states decrease. And finally, the sum rule values are exhausted by the transitions to resonances.

This paper, being the third part of our studies, sheds light on the separation of the strength function related to the cross section by using ECR with CSM. Description of the strength function on the real energy axis in terms of bound, resonance and continuum states is performed by applying ECR to the Green function. Berggren et al.[13),15)−17)] have discussed this problem but they restricted themselves to see the effects from bound and resonance terms, not from continuum one. It is, therefore, meaningful to examine the explicit contributions from these three kinds of states in the strength function. The analysis of these three components will bring us a deeper understanding of the excitation mechanism of the system. For example, in the view of an actual system, the observed transition strengths in the Coulomb breakup reactions of some neutron-rich nuclei such as ^{11}Be[18)] and ^{11}Li[19),20)] show the enhancement at the low energy region and it is needed to clarify which kind of states determines the observed behavior.

In the next section (§2), we briefly explain the way of separation using ECR with CSM, and apply it to the schematic potential model which is the same as we have employed in previous papers.[11),12)] In §3, we investigate and discuss the problem of breakup mechanism of ^{11}Be, and show the present method works well in the actual system. The section §4 is devoted to the discussion about the separation of the $E2$ strength function of the ^{16}O+α system. Summary is given in §5.

§2. The strength function in CSM

Applying ECR to the calculations of any physical quantities allows us to see the contributions from bound, resonance and continuum states to them. Berggren et al.[13),15)] have discussed the separation of the strength function into the three terms by introducing various types of ECR in which the patterns of separation of the states into three terms are different each other. However, they restricted the discussion to the investigation of the validity of each type of the pole expansion and did not explicitly examine the continuum term which is a residual part of the pole expansion. Then it is necessary to have a more complete discussion with taking into account the continuum term. As will be shown below, CSM enable us to introduce ECR uniquely, and see the explicit contributions of three kinds of states in the strength function.

In the next subsection, we formulate the way of the separation of the strength function using CSM, and as an example, an application to a schematic potential model is done in the second subsection. The detailed procedures of the calculational way of matrix elements in CSM are given in our previous papers,[11),12)] and so we skip them here.

2.1. *Separation of the strength function into bound, resonance and continuum terms*

A strength function $\mathcal{S}(E)$ is expressed by using the response function $R(E)$ as

$$\mathcal{S}_\lambda(E) = \sum_\nu \langle \Phi_i | \widehat{O}_\lambda^\dagger | \Phi_\nu \rangle \langle \Phi_\nu | \widehat{O}_\lambda | \Phi_i \rangle \delta(E - E_\nu) \tag{1}$$

$$= -\frac{1}{\pi} \mathrm{Im} R_\lambda(E), \tag{2}$$

$$R_\lambda(E) = \int d\boldsymbol{r} d\boldsymbol{r}' \, \Phi_i^*(\boldsymbol{r}) \, \widehat{O}_\lambda^\dagger \, \mathcal{G}(E, \boldsymbol{r}, \boldsymbol{r}') \, \widehat{O}_\lambda \, \Phi_i(\boldsymbol{r}'), \tag{3}$$

where E is an energy on a real axis, $|\Phi_i\rangle$, $|\Phi_\nu\rangle$ and $\widehat{O}_\lambda$ are initial, final states and an arbitrary transition operator with rank λ, respectively. E_ν are energies of the final state. In this expression, we assume the bound (initial) and final states to construct a complete set of the Hamiltonian H;

$$\sum_{\nu(i)} |\psi_\nu\rangle\langle\psi_\nu| = \mathbf{1}, \tag{4}$$

where summation includes the initial state (i) as a member of the complete set.

A general expression of the completeness relation proposed by Berggren et al.[13),15)] is called the "extended completeness relation" (ECR) because of the explicit decomposition of scattering (unbound) states into resonance and residual continuum ones;

$$\sum_B^{n_B} |\Phi_B\rangle\langle\widetilde{\Phi}_B| + \sum_R^{n_R(L)} |\Phi_R\rangle\langle\widetilde{\Phi}_R| + \int_L dk |\Phi_k\rangle\langle\widetilde{\Phi}_k| = \mathbf{1}, \tag{5}$$

where B denotes bound states with momentum k_B obtained as poles on the upper-half imaginary axis and R resonances with k_R obtained in the region surrounded

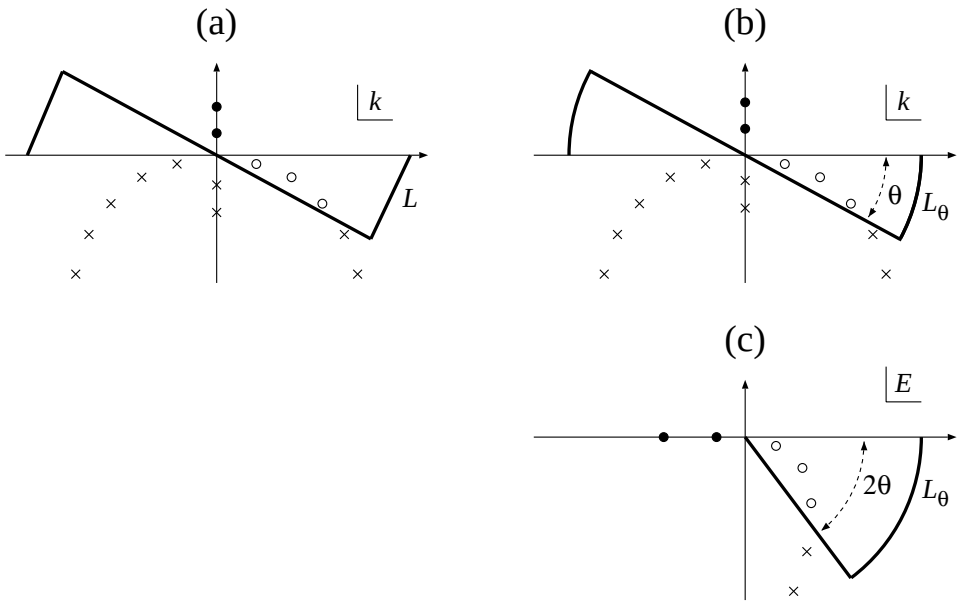

Fig. 1. The two upper figures (a) and (b) are schematic illustrations of an S-matrix pole distribution with integral contour which presents a rotated cut of the Riemann plane (thick line) in the complex momentum plane. The contour L of (a) is one of the four types (L, U, W and Z) proposed by Berggren et al.,[15] and L_θ of (b) corresponds to the case of CSM. The solutions of bound states are presented with solid circles and obtainable resonances are open circles. Hidden poles which cannot be solved with integral contour L or L_θ are also shown by crosses. Figure (c) is the corresponding pole solutions in CSM in the complex energy plane.

by the real axis and a contour L in the complex momentum plane as shown in Fig. 1(a), where contour L is one of the choices for the separation of scattering states into resonance and continuum states. The number of bound and resonance states are given by n_B and $n_R(L)$, respectively. The continuum states with a complex momentum k are defined by the solutions on the contour L. The bra-states with tilde indicate the bi-orthogonal ones of their ket-states. For discrete states (bound and resonance), $\tilde{k}_P = -k_P^*$ $(P = B, R)$ and for other continuum states, $\tilde{k} = k^*$.[13]

To calculate the matrix elements with ECR, we must prepare the solutions of resonances and continuum states for a given contour L in addition to the bound state solutions. Such a separation of the scattering states and construction of ECR in the many-body Hamiltonian can be done by using CSM. In CSM, an integral contour for the continuum states is chosen to be L_θ formed by a straight line rotated down by θ from the real axis and semi-circles between the real axis and the straight θ line in the complex momentum plane as shown in Fig. 1(b). On the complex energy plane, this θ line is expressed by a 2θ line in the forth (and possibly third) quadrant as shown in Fig. 1(c). Therefore, ECR with the solutions of the complex scaled Hamiltonian

$H(\theta)$ in CSM is expressed as

$$\sum_{B}^{n_B} |\Phi_B^\theta\rangle\langle\widetilde{\Phi}_B^\theta| + \sum_{R}^{n_R(L_\theta)} |\Phi_R^\theta\rangle\langle\widetilde{\Phi}_R^\theta| + \int_{L_\theta} dk_\theta |\Phi_{k_\theta}^\theta\rangle\langle\widetilde{\Phi}_{k_\theta}^\theta| = \mathbf{1}, \tag{6}$$

where k_θ is a momentum given along L_θ and energy is expressed as $E_\theta = \hbar^2 k_\theta^2/2\mu$. When $\theta = 0$, $n_R(L_\theta)$ is zero and L_θ is the real axis of momentum and energy, and continuum states correspond to scattering ones (for detail, see Ref.12)).

Using the complex scaled initial wave functions Φ_i^θ, Hamiltonian $H(\theta)$ and transition operator $\widehat{O}_\lambda^\theta$, the response function is expressed as

$$R_\lambda(E) = \int d\boldsymbol{r} d\boldsymbol{r}'\, \widetilde{\Phi}_i^{\theta\,*}(\boldsymbol{r})\, (\widehat{O}_\lambda^\dagger)^\theta\, \mathcal{G}^\theta(E, \boldsymbol{r}, \boldsymbol{r}')\, \widehat{O}_\lambda^\theta\, \Phi_i^\theta(\boldsymbol{r}'), \tag{7}$$

where the complex scaled Green function is written as

$$\mathcal{G}^\theta(E, \boldsymbol{r}, \boldsymbol{r}') = \langle \boldsymbol{r}| \frac{\mathbf{1}}{E - H(\theta)} |\boldsymbol{r}'\rangle. \tag{8}$$

Here, it is worthwhile to notice that $R_\lambda(E)$ is invariant on the scaling. Substituting Eq. (6) into Eq. (8), we can separate the Green function into three terms,

$$\begin{aligned}\mathcal{G}^\theta(E, \boldsymbol{r}, \boldsymbol{r}') = &\sum_{B}^{n_B} \frac{\Phi^\theta(\boldsymbol{r}, k_B)\, \widetilde{\Phi}^{\theta\,*}(\boldsymbol{r}', k_B)}{E - E_B} + \sum_{R}^{n_R(L_\theta)} \frac{\Phi^\theta(\boldsymbol{r}, k_R)\, \widetilde{\Phi}^{\theta\,*}(\boldsymbol{r}', k_R)}{E - E_R} \\ &+ \int_{L_\theta} dk_\theta \frac{\Phi^\theta(\boldsymbol{r}, k_\theta)\, \widetilde{\Phi}^{\theta\,*}(\boldsymbol{r}', k_\theta)}{E - E_\theta},\end{aligned} \tag{9}$$

where E_B and $E_R (= E_r - \frac{i}{2}\Gamma)$ are the energy eigenvalues of bound and resonance states, respectively. From Eq. (7), we obtain the following relations for the response function.

$$R_\lambda(E) \;=\; R_{\lambda,B}(E) + R_{\lambda,R}^\theta(E) + R_{\lambda,k}^\theta(E), \tag{10a}$$

$$R_{\lambda,B}(E) \;= \sum_{B}^{n_B} \frac{\langle\widetilde{\Phi}_i^\theta|(\widehat{O}_\lambda^\dagger)^\theta|\Phi_B^\theta\rangle\langle\widetilde{\Phi}_B^\theta|\widehat{O}_\lambda^\theta|\Phi_i^\theta\rangle}{E - E_B}, \tag{10b}$$

$$R_{\lambda,R}^\theta(E) \;= \sum_{R}^{n_R(L_\theta)} R_\lambda(r, E), \;\; R_\lambda(r, E) = \frac{\langle\widetilde{\Phi}_i^\theta|(\widehat{O}_\lambda^\dagger)^\theta|\Phi_R^\theta\rangle\langle\widetilde{\Phi}_R^\theta|\widehat{O}_\lambda^\theta|\Phi_i^\theta\rangle}{E - E_R}, \tag{10c}$$

$$R_{\lambda,k}^\theta(E) \;= \int_{L_\theta} dk_\theta \frac{\langle\widetilde{\Phi}_i^\theta|(\widehat{O}_\lambda^\dagger)^\theta|\Phi_{k_\theta}\rangle\langle\widetilde{\Phi}_{k_\theta}|\widehat{O}_\lambda^\theta|\Phi_i^\theta\rangle}{E - E_\theta}. \tag{10d}$$

and the strength function is similarly separated as

$$\mathcal{S}_\lambda(E) = \mathcal{S}_{\lambda,B}(E) + \mathcal{S}_{\lambda,R}^\theta(E) + \mathcal{S}_{\lambda,k}^\theta(E). \tag{11}$$

Matrix elements of the scaled operator are independent of θ, if the scaled wave functions are solved with the same θ. Therefore, the θ-dependence of $R_{\lambda,R}^\theta(E)$ and $R_{\lambda,k}^\theta(E)$ comes from only $n_R(L_\theta)$ and E_θ (dk_θ), respectively.

CSM allows us to calculate each term of Eq. (11) easily because bound and resonance states are obtained under the same boundary conditions, and continuum states are on the contour L_θ determined by θ uniquely.[12] These points of CSM are quite advantageous in comparison with other methods. Now as we are interested in the energy above threshold, we drop the bound state term in Eq. (11), and the strength function is expressed by two terms of resonance and continuum states. In an actual calculation, integration over momentum or energy for the continuum term is limited to a finite value on the straight line of L_θ in which residual contribution from the semi-circle of L_θ is negligible.

2.2. *Application to the schematic potential model*

We here take a simple schematic potential problem[21] to show a reliability of the present method, and investigate how the strength function is separated into the terms in Eq. (11). The parameter set of the schematic potential model is given as follows:

$$H = T + V(r), \quad T = -\frac{\hbar^2}{2\mu}\nabla^2, \quad V(r) = V_1 e^{-\mu_1 r^2} + V_2 e^{-\mu_2 r^2}, \tag{12}$$

where we put $\hbar^2/\mu = 1$ MeV·fm^2 for simplicity and $V_{1,2} = -8.0$ MeV, 4.0 MeV and $\mu_{1,2} = 0.16$ fm^{-2}, 0.04 fm^{-2}, respectively. Eigenvalues of bound and resonance states for $J^\pi = 0^+$, 1^- are calculated by diagonalizing the complex scaled Hamiltonian $H(\theta)$. As shown in Fig. 2, one bound and nine resonance solutions for the $J^\pi = 1^-$ states are obtained at the scaling angle $\theta \simeq 45°$.

In this paper, we investigate the dipole transition from the ground state of 0^+ ($E_{\text{g.s.}} = -1.92$ MeV) to 1^- states for the operator defined by

$$\widehat{O}_1 = rY_{10}(\hat{\boldsymbol{r}})\sqrt{4\pi}, \tag{13}$$

where r is a relative distence of two-body system.

As far as we consider a simple two-body case with a potential such as Eq. (12), we can calculate the strength function using scattering states solved with a standard technique, without introducing special procedure like CSM. However, it is nothing but a special case of CSM in which θ=0°, $n_R(L_{\theta=0}) = 0$ and the (rotated-)continuum line is existing on a positive real energy axis.

In Fig. 3 we show the dipole transition strength function from $0^+_{\text{g.s.}}$ to the scattering states of 1^-. The upper panel shows the whole shape in a log scale and the lower an enlarged figure in a linear scale. We can see the distinct structure in the distribution and speculate that the sharp peak at 1.17 MeV comes

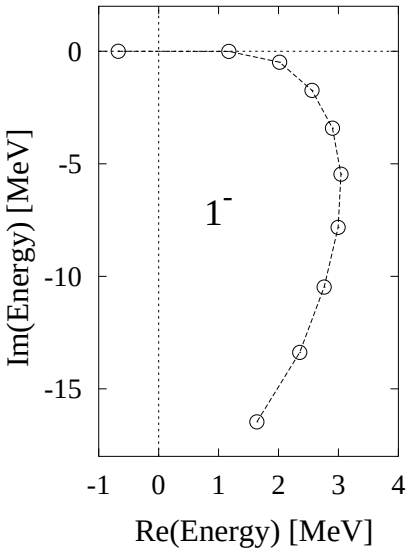

Fig. 2. Complex energy eigenvalue distribution obtained with CSM for 1^- states.

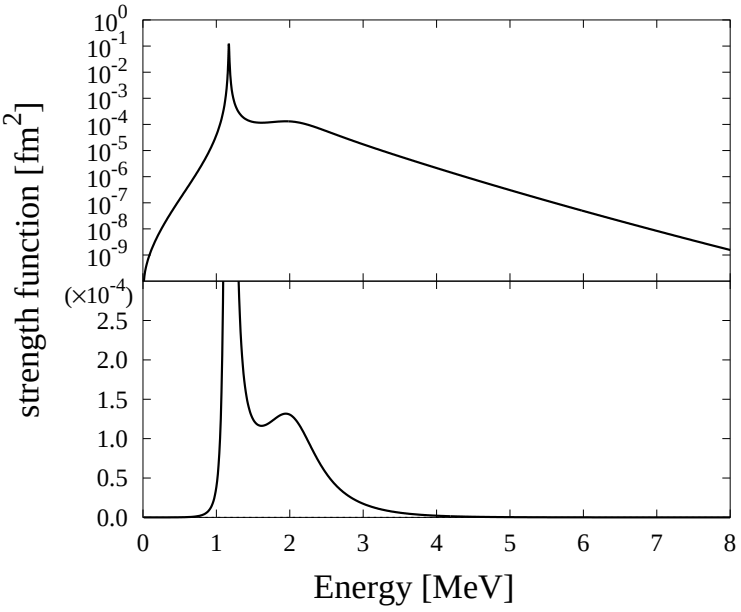

Fig. 3. Dipole strength function ($0^+ \to 1^-$) calculated by using scattering solutions in the schematic potential model. The upper panel is given in a log scale and lower enlarged figure in a linear scale.

from the first 1^-resonance state which is a quasi-bound one, and the shoulder around 2 MeV is from the second resonance solved above the potential barrier. By separating the strength function obtained using scattering solutions into resonance and continuum terms, we can get more resolved understanding of the structure.

In Fig. 4, we show the results of the separation calculated with two different scaling angles $\theta = 3^\circ$ (left figure) and 10° (right figure). Dashed and dash-dotted lines mean the contributions from the first and second resonances respectively, and dotted lines correspond to those from continuum states specified by θ. Solid lines are the sums of the contributions from each term and in good agreement with the strength function using the scattering solutions at θ=0° and shown by open circles.

From Fig. 5 which shows the position of the resonance poles in the complex energy plane, for the scaling angle $\theta = 3^\circ$, we obtain only one 1^- resonance at $\theta_R = \frac{1}{2}\tan^{-1}(\Gamma/2E_r)$=0.12° in the complex energy plane, and for $\theta = 10^\circ$, we obtain the second 1^- resonance at θ_R =6.78° in addition to the first one. Therefore in Fig. 4, at $\theta = 3^\circ$, the shoulder of the strength function around 2 MeV is described by the strength to the continuum states, and when we increase the scaling angle over θ_R = 6.78°, the second resonance appears and its contribution to the strength function is separated from the continuum term. This result indicates that the separation of the strength function is successfully done at any θ.

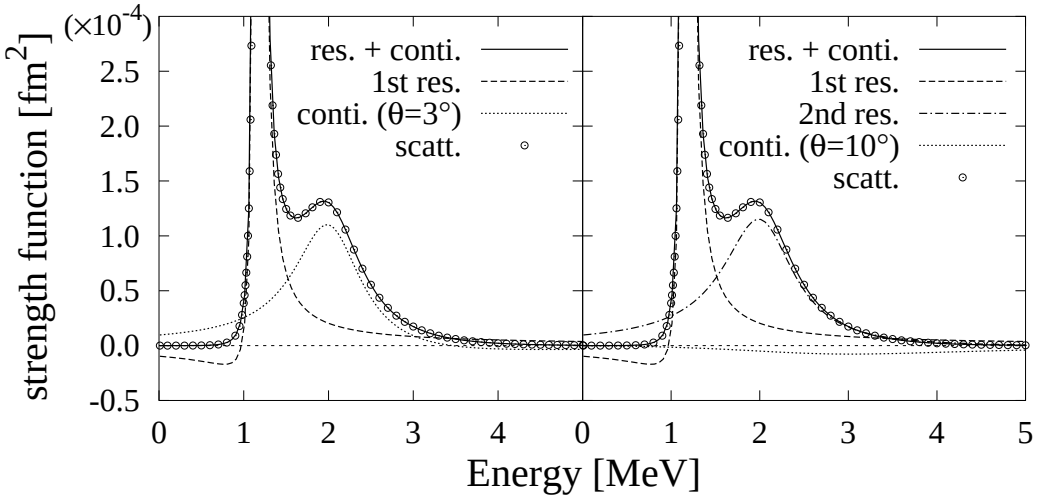

Fig. 4. Contents of the dipole strength function ($0^+ \to 1^-$) at θ=3° (left) and 10° (right) in the schematic potential model. Dashed and dash-dotted lines show the components of the first and second resonances, respectively, and the dotted line is the continuum term. Solid lines present a sum of the contributions from resonance and continuum states. Open circles are the calculated results using the scattering solutions shown in Fig. 3.

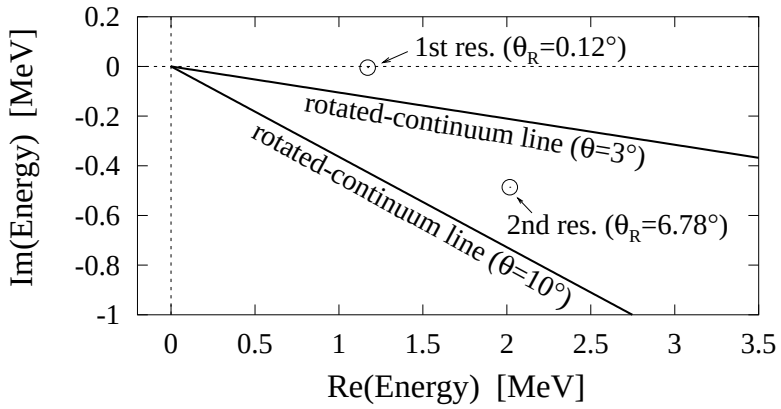

Fig. 5. Position of the first and second resonances of 1^- states with rotated-continuum lines at θ=3° and 10° in the schematic potential model.

It should be noticed that the sign of the strength function of each component is not always positive. For example, the first resonance gives the negative strength in the region where energy is less than 1 MeV and the continuum term at $\theta = 3°$ and the second resonance term at $\theta = 10°$, cancel out this negative contribution to let the sum of strength be positive totally. This behavior is quite interesting and will be discussed in the following section again.

From the right-side of Fig. 4, we can confirm the fact that the contribution from continuum term is very small and that the two resonances construct the main structure of the dipole strength function. Then it is expected that the strength

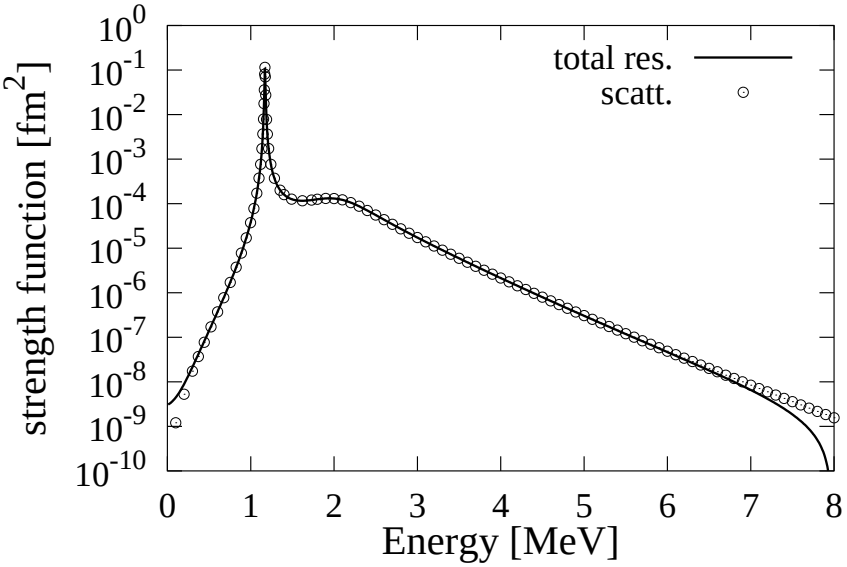

Fig. 6. Dipole strength function ($0^+ \to 1^-$) to the only 1^- resonance states obtained in the 4th quadrant region of complex energy plane with CSM. Open circles are the same distribution as shown in the upper panel of Fig. 3.

function can be expressed by means of only resonance terms. As was mentioned in a previous paper,[12] the sum rule value of dipole transitions in this model is almost exhausted by resonance states.

In Fig. 6, we show the distribution from resonances obtained in the 4th quadrant shown in Fig. 2. We can see that the strength function formed by a sum of the resonance terms is in good agreement with the one using scattering solutions and the difference is at most around 10^{-8} fm^2 which corresponds to the continuum term. This means that the assumption of pole expansion of the strength function is quite well established in this case.

§3. Coulomb breakup of ^{11}Be into ^{10}Be+n

We apply our method to a typical one-neutron halo nucleus ^{11}Be. Many works have been published until today[18),22)−30)] about the halo structure of this nucleus. One of the main interests is why level inversion of $1s_{1/2}$ and $0p_{1/2}$ states occurs[27)−30)] and another interest is how to explain the mechanism of the Coulomb breakup reaction[18),24)−26)] into ^{10}Be and a neutron in association with the possibility of the soft dipole resonance. The dipole strength distribution function of this reaction has been observed by Nakamura et al.[18)] and their analysis shows a strong enhancement of the strength at the low energy. Using a plane wave approximation, they interpreted that the breakup process was "direct" but not through any resonances. The low energy enhancement in the distribution has been explained by a halo structure of

the ground state. However, it is necessary to perform a more precise analysis with no assumption such as a plane wave approximation, for an understanding of the breakup mechanism.

Here, we concentrate our attention to the problem whether the dipole strength function observed in the breakup reaction with low energies has any contributions from resonances or not. For this purpose, we employ a simple ^{10}Be+n model, assuming that ^{10}Be is described by the spherical shell model configuration with a p-shell closed for neutrons: $(0s_{1/2})^4(0p_{3/2})^6$. More realistic model calculations taking into account the deformation of the core nucleus ^{10}Be will be carried out elsewhere. As an interaction between the core nucleus and valence neutron, the potential of a folding type[6] is employed by using the so-called Modified-Hasegawa-Nagata (MHN) force as the effective nucleon-nucleon potential. The Hamiltonian of this system is given as

$$H = T + V_{\rm f}, \quad T = -\frac{\hbar^2}{2\mu}\nabla^2, \quad V_{\rm f} = V_{\rm c} + V_{\rm ls}, \tag{14}$$

where μ and $V_{\rm f}$ are the reduced mass between ^{10}Be and neutron and the folding-type potential expressed by a sum of the folding central potential $V_{\rm c}$ and the density-derivative ls potential $V_{\rm ls}$. In fact, due to the simple description of the core nucleus ^{10}Be, the calculated energy levels do not fit the experimental ones. Then we introduce one adjustment parameter in the nucleon-nucleon potential to fit the experimental energy levels of two bound states $\frac{1}{2}^+$ and $\frac{1}{2}^-$ of ^{11}Be. For the positive parity states, the strength of the second range of the MHN potential is enhanced by about 15% and for the negative parity states, it is slightly reduced by 0.6%. Of course the frozen core without any effects of excitation and deformation is unsuitable for describing the realistic ^{10}Be nucleus, however, we here emphasize that what we want to see is the roles of resonance and continuum states and that the obtained results may give us a new understanding for the breakup mechanism.

Now as we are interested in the dipole transition, we calculate the reduced transition probability to the first excited state ($\frac{1}{2}^-$), $B(E1;\frac{1}{2}^+ \to \frac{1}{2}^-)$, and the dipole strength function to the scattering states ($J^\pi_f = \frac{1}{2}^-, \frac{3}{2}^-$), $dB(E1;\frac{1}{2}^+ \to J^\pi_f, E)/dE$, which are defined as follows:

$$B(E1;\tfrac{1}{2}^+ \to \tfrac{1}{2}^-) = \sum_{M_f,m} \langle \widetilde{\Phi}_{\frac{1}{2}^+} | \widehat{O}^\dagger_m(E1) | \Phi_{\frac{1}{2}^-,M_f} \rangle \langle \widetilde{\Phi}_{\frac{1}{2}^-,M_f} | \widehat{O}_m(E1) | \Phi_{\frac{1}{2}^+} \rangle, \tag{15}$$

$$\frac{dB(E1;\frac{1}{2}^+ \to \frac{1}{2}^-, \frac{3}{2}^-, E)}{dE} = \sum_{\substack{J^\pi_f = \frac{1}{2}^-, \frac{3}{2}^- \\ M_f,m}} \langle \widetilde{\Phi}_{\frac{1}{2}^+} | \widehat{O}^\dagger_m(E1) | \Phi_{J^\pi_f,M_f}(E) \rangle \langle \widetilde{\Phi}_{J^\pi_f,M_f}(E) | \widehat{O}_m(E1) | \Phi_{\frac{1}{2}^+} \rangle, \tag{16}$$

where $\widehat{O}_m(E1) = -e(Z_c/A)rY_{1m}(\hat{\boldsymbol{r}})$, and Z_c, A and r are the charge of the core nucleus ^{10}Be, the mass number and the relative distance between ^{10}Be and a neutron, respectively. The wave function of ^{11}Be is expressed by Φ_{J^π,M_f}. We first discuss the

Table I. Results of the calculated r.m.s. radius and $B(E1)$ to the first excited state in ^{11}Be in comparison with other theoretical calculation[30] and experimental data.[22)–24)]

	r.m.s. radius [fm]	B(E1;$\frac{1}{2}^+ \to \frac{1}{2}^-$) [$e^2$fm^2]
cal.	2.93	0.271
GCM[30]	2.69	0.163
exp.	2.73±0.05[23]	0.116±0.012[22] 0.100±0.015[24]

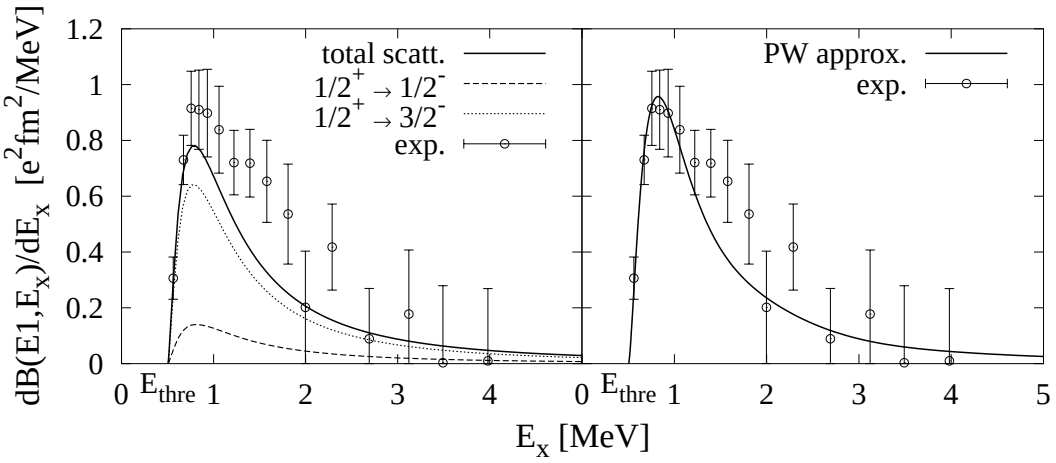

Fig. 7. Dipole strength functions calculated by using scattering solutions (left) and plane wave approximation (right). Dashed and dotted lines show the contribution of $1/2^+ \to 1/2^-$ and $3/2^-$, respectively. The total transitions are presented by the solid line. Open circles with errorbars are experimental data.[18)]

reliability of the present ^{10}Be+n model by calculating several physical quantities, and next search for poles of excited states of ^{11}Be in order to examine the effects of resonance and continuum states on the strength function.

Table I shows the calculated r.m.s. radius and $B(E1; \frac{1}{2}^+ \to \frac{1}{2}^-)$ in comparison with other theoretical and experimental results. In the GCM model,[30] the core excitation is included and a parity dependent potential is adopted like that in our model. We can see the differences between the present and other calculations for both r.m.s radius and $B(E1)$. This may be due to a lack of d-wave components in the description of the ground state ($\frac{1}{2}^+$) of ^{11}Be in our model. The strong $E1$ transition to the first excited state indicates that the overlapping between initial and final states is too large.

In Fig. 7, we show the dipole strength functions to the scattering states of $\frac{1}{2}^-$ and $\frac{3}{2}^-$, comparing two calculations with using a scattering solutions (left-hand side) and a plane wave approximation (right-hand side). In a plane wave approximation, the transition to the first excited state is excluded by taking into account the orthogonality between the plane wave and the first excited state. We can see a good

agreement with the experimental data as well as other authors insist.[18),25),26)] The strength function obtained by using scattering solutions shows the similar shape as that of plane wave approximation. However, the magnitude is slightly less than the experimental data because of a strong transition to the first excited state of ^{11}Be.

Next, we discuss the contribution of resonances to the dipole strength function. In Fig. 8, we show the pole distribution of the final states $\frac{1}{2}^-$ and $\frac{3}{2}^-$ in ^{11}Be at the scaling angle $\theta = 37.4°$. In the present model, low energy resonance poles are not found, but there are resonances with energies higher than 10 MeV and decay widths larger than 60 MeV. Although there may exist other resonance poles, we include them in the continuum term because they have large widths and cannot be considered as physical resonances.

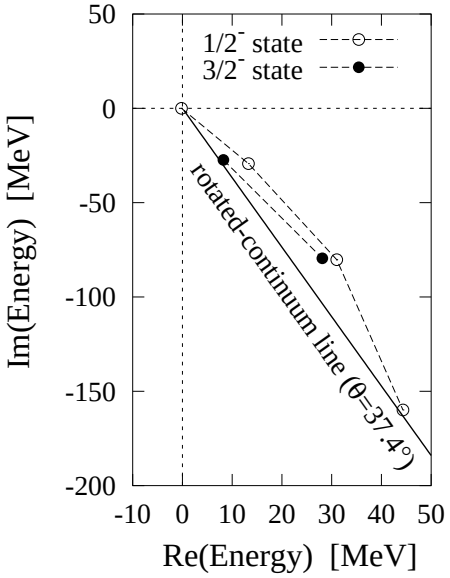

Fig. 8. Pole distributions of $1/2^-$ and $3/2^-$ states obtained with CSM in the complex energy plane. The continuum line is rotated down by $2\theta = 74.8°$.

Before separating the dipole strength function shown in the left-hand side of Fig. 7, we investigate the contributions from bound, resonance and continuum states to the energy weighted sum rule value. The sum rule value $S_1(E\lambda, J_f^\pi)$ is defined as follows

$$S_1(E\lambda, J_f^\pi) = \sum_\alpha (E_{J_f^\pi,\alpha} - E_{J_i}) \times B(E\lambda; J_i \to J_f^\pi, \alpha). \tag{17}$$

The calculated sum rule values using the solutions of bound and scattering states are $S_1(E1, \frac{1}{2}^-) = 2.62\ e^2\text{fm}^2\text{MeV}$ and $S_1(E1, \frac{3}{2}^-) = 3.17\ e^2\text{fm}^2\text{MeV}$, respectively. In Table II, we show the contribution of bound, resonance and continuum states to the

Table II. Sum rule values of the $E1$ transition ($1/2^+ \to 1/2^-, 3/2^-$) at $\theta = 37.4°$. All values are represented in the unit of $S_1(E1, 1/2^-) = 2.62e^2\text{fm}^2\text{MeV}$ for the $1/2^-$ states and of $S_1(E1, 3/2^-) = 3.17e^2\text{fm}^2\text{MeV}$ for the $3/2^-$ states. Last row presents sums of each term.

	$J_f^\pi = \frac{1}{2}^-$		$J_f^\pi = \frac{3}{2}^-$	
	real	imaginary	real	imaginary
bound	0.1001	0.0000	—	—
1st resonance	0.5189	0.2869	0.2642	0.4051
2nd resonance	−0.2289	0.2263	−0.1716	0.0211
3rd resonance	0.3493	−0.2595	—	—
continuum	0.2616	−0.2540	0.9079	−0.4254
total	1.0009	−0.0003	1.0005	0.0008

sum rule values at $\theta = 37.4°$. Although the total values in the last row of Table II should be unity, small deviations are seen and considered to be due to a numerical error. Therefore, we think that ECR is well satisfied and the obtained results are consistent enough to evaluate the contributions from each state.

Those results lead us to the following views: i) Every state contributes comparably to the sum rule value. The sum rule value is not exhausted by specific bound and resonance states. ii) Therefore, the strength function is not considered to be explained by the pole expansion in terms of resonances, in contrast to the case discussed in §2.2. We need to investigate the contributions from continuum states together with those from resonances. iii) The sum rule value of each state is not always positive, for example, the second resonance term of $\frac{1}{2}^-$ has a minus sign of the real part and gives a negative contribution to the sum rule value. Since the bra-states are not the complex conjugate of ket-states in ECR of Eq. (5), it is not necessarily kept that contributions from every term are always positive. In this case, since the resonance pole expansion of the sum rule value does not converge in a monotonic way, we cannot generally say that resonance states "exhaust" the sum rule value within the limits of a finite number of resonances.

By using these bound, resonance and continuum states, the dipole strength function is separated into corresponding terms as well as we did in § 2.2. The calculated result is shown in Fig. 9, where the upper panel presents the resonance term and the lower continuum one. The resonance term contains the contributions from five resonance states shown in Fig. 8 and we can easily recognize that its effect is negligible. It is therefore very hard to find out the difference between the continuum term and the distribution shown in the left-hand side of Fig. 7. This indicates that as long as we are discussing the $E1$ transition with the model Hamiltonian adopted here, the Coulomb breakup of ^{11}Be is caused directly but not through specific resonances.

As we have shown in Table II, the contribution of each resonance state to the energy weighted sum rule value is not so small. Then the results of the strength function seem to contradict to those of the sum rule value. However, the sum rule values defined by the energy-weighted transition matrices are enhanced for resonance states with large resonance energies and decay widths. On the other hand, from Eq. (10c), the response function is defined as the matrix elements divided by the energy in contrast to the case of the sum rule value. From the different energy dependence of the sum rule value and the strength function, we can understand why resonance states obtained here hardly contribute to the strength function, but give large contribution to the sum rule value.

Thus, we can now say that the interpretation about the breakup mechanism of ^{11}Be proposed by Nakamura et al.[18] is right. At least the enhanced peak of the strength function at low energy is caused through a direct breakup and indicates the spatially extended wave function of the ground state of ^{11}Be. Some experimental data,[31] however, indicate the existence of a few energy levels concerning with the $E1$ transition strength. Although the interpretation about the breakup mechanism may not be changed, it is worthwhile to check the effects of low energy resonances in a more sophisticated model.

§4. Discussion

In previous sections §2.2 and §3, we have discussed the schematic potential model and the more realistic ^{10}Be+n model to show the feasibility of our method. The former model shows that the strength function is almost reproduced by resonances as well as for the sum rule value.[11),12)] On the other hand, the latter model shows that any resonances do not give a dominant contribution to the strength function. In these two cases, the strengths concentrate on either resonance or continuum states dominantly. In this section, we discuss another example of the ^{16}O+α model for ^{20}Ne, which corresponds to the intermediate situation where both resonance and continuum states contribute to the strength function equally well. We solve bound, resonance and continuum states applying CSM to the orthogonality condition model (OCM) of ^{16}O+α,[5)] and calculate the $E2$ transition strength $dB(E2)/dE$ between

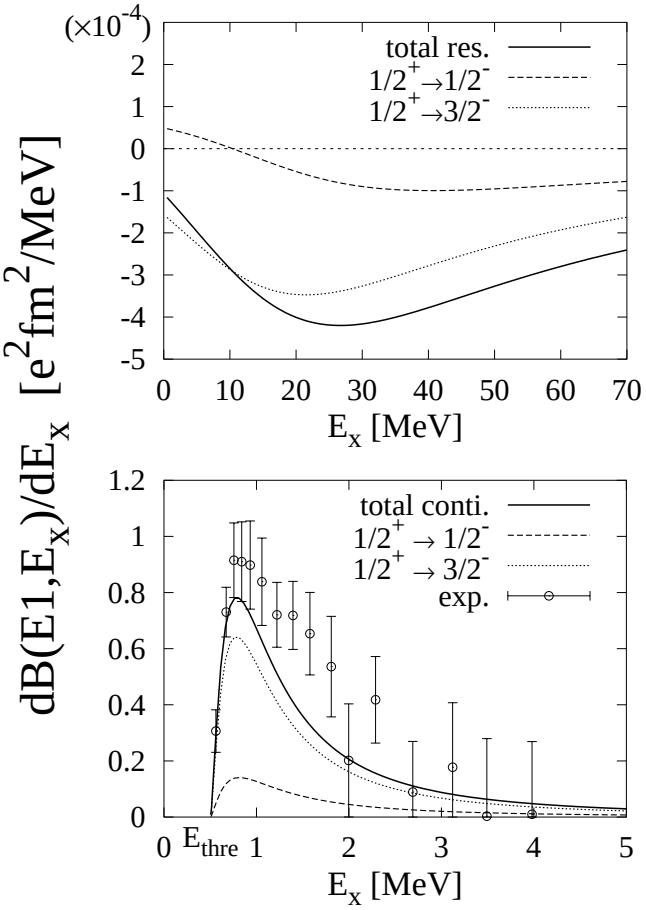

Fig. 9. Separation of the dipole strength function into resonance (upper) and continuum (lower) terms at $\theta = 37.4^\circ$. Dashed, dotted and solid lines correspond to the transition for $1/2^+ \to 1/2^-, 3/2^-$ and total, respectively. Open circles with errorbars are the experimental data.

the ground band state ($K^\pi = 0_1^+$) and 2^+ state including the higher nodal ($K^\pi = 0_4^+$) band in ^{20}Ne. The Hamiltonian of the ^{16}O+α OCM is given as follows;

$$H = -\frac{\hbar^2}{2\mu}\nabla^2 + V, \quad V = V_N + V_C, \tag{18}$$

$$V_N = V_0 e^{-\nu_n r^2}, \quad V_C = 8 \cdot 2\frac{e^2}{r}\mathrm{erf}(\nu_c r), \tag{19}$$

where μ is a reduced mass and V_0, ν_n, ν_c are -154 MeV, 0.1102 fm^{-2} and 0.4805 fm^{-1}, respectively. The obtained energies and decay width of 0_1^+ (ground state) and 2_4^+ (resonance) are $E(0_1^+) = -4.15$ MeV and $E(2_4^+) = 4.21$ MeV from a threshold of ^{16}O+α and $\Gamma = 3.10$ MeV (θ_R=9.84°), respectively. It is noted that the associated resonance state 2_4^+ has a decay width comparable to its resonance energy. The operator of the $E2$ transition is given as

$$\widehat{O}_m(E2) = \frac{e}{2}\frac{16}{5}r^2 Y_{2m}(\hat{\boldsymbol{r}}), \tag{20}$$

where r is the relative distance between ^{16}O and α. The contribution from the 2_4^+ state to the sum rule value of the $E2$ transition is 39.5% for the real part and -74.5% for the imaginary in a unit of the total real value. In this case, the resonance component shows the negative sign in the imaginary part as well as the ^{11}Be case.

In Fig. 10, we show the separation of the $dB(E2)/dE$ into the 2_4^+ resonance term (dashed line) and the continuum term (dotted line) at a scaling angle θ=15°. A sum of the two terms (solid line) is in good agreement with the distribution obtained by using scattering solutions (open circles).

It is easily found that the peak of the $E2$ transition strength function is mainly constructed by the resonance term, and the remained part is restored by the continuum one. The resonance term of the strength function makes a peak at around 5 MeV in spite of that the resonance energy is a little bit lower than this value. This means that the position of the peak in the strength function is not always the same as the resonance energy due to the relatively large decay width and the imaginary part of the matrix element concerning with the resonance state. As the decay width of the resonance state is reduced and the associated matrix element of the state is almost real number, the position of the peak in the strength function becomes closer to the resonance energy. In such a case, the Breit-Wigner formula is applicable (See Eq. (10c)).

Although each term of the strength function has not only positive but also negative values, a sum of the each contribution becomes positive in all energy regions. The problem of the sign of the transition strength is not figured out and its interpretation is still an open problem.

§5. Summary

Since unbound states are expected to play an essential role in unstable nuclear physics, we have to know as much information associated with these states as possible. Besides calculating resonance energies and decay widths, it is necessary to

make a framework which enables us to examine the effect of resonances on the real observed physical quantities directly. By using the extended completeness relation in the framework of the complex scaling method, we performed the separation of the transition strength function into bound, resonance and continuum terms. Using the obtained method, we can investigate the structure in the cross section and the excitation mechanisms of various systems in detail.

Applications of the present method to the actual nucleus are also performed in addition to the schematic potential model. We examined the reliability of the present method through the successful results of these model. The advantageous points of the present method are summarized as i) bound, resonance and continuum solutions which construct a basis set of ECR can be easily obtained with CSM, and ii) especially the contributions from the continuum states obtained on the rotated branch cut L_θ can be calculated without any ambiguities about the selection of an integral contour.

For ^{11}Be, within a simple ^{10}Be+n potential model, the Coulomb breakup mechanism is analyzed without any assumption such as a plane wave approximation. The present calculation explicitly shows the contributions both from resonances and from continuum states. And the interpretation of the direct breakup is justified. For the ^{20}Ne system, a clear separation of the $E2$ transition strength can be seen. It is shown that the present method has large flexibility and applicability to various systems.

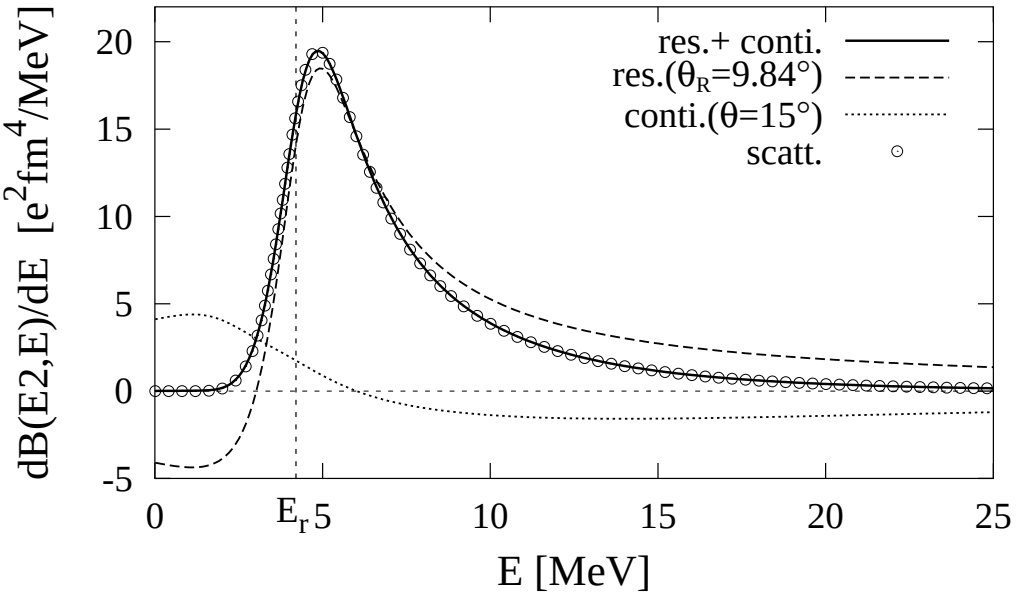

Fig. 10. Separation of $dB(E2;0^+ \to 2^+,E)/dE$ into resonance (2^+_4) and continuum terms with comparison to the one obtained by using scattering solutions at $\theta = 15^\circ$. A sum of the resonance and continuum terms is shown by solid line. Vertical thin dashed line shows a position of the resonance energy of 2^+_4 state.

The sign of the strength function and of the sum rule values are still important and provide us with interesting problems for further studies.

While we restricted ourselves to the application of the method formulated in the paper to two-body systems, more theoretical developments including multi-channel and many-body cases are expected to be done naturally. It will bring us the wider understanding of the breakup mechanism, for example, for the two-neutron halo nucleus ^{11}Li. The present results are instructive enough to tell us the direction to answer them.

Acknowledgements

The authors would like to thank the members of the theoretical nuclear group in Hokkaido University for their kind interest and valuable discussions. This work was supported by the Grant-in-Aid for Scientific Research (No. 8213201 and No. 08640340) of the Ministry Education, Science and Culture (Japan).

References

1) I. Tanihata, Nucl. Phys. **A488** (1988), 113c.
2) K. Ikeda, Nucl. Phys. **A538** (1992), 355c.
3) J. Aguilar and J.M. Combes, Commun. Math. Phys. **22** (1971), 269.
E. Balslev and J.M.Combes, Commun. Math. Phys. **22** (1971), 280.
4) A. T. Kruppa, R.G. Lovas and B. Gyarmati, Phys. Rev. **C37** (1988), 383.
5) A. T. Kruppa and K. Katō, Prog. Theor. Phys. **84** (1990), 1145.
6) K. Katō and K. Ikeda, Prog. Theor. Phys. **89** (1993), 623.
7) A. Csótó, Phys. Rev. **C49** (1994), 3035.
8) S. Aoyama, S. Mukai, K. Katō and K. Ikeda, Prog. Theor. Phys. **93** (1995), 99; **94** (1995), 343.
9) K, Katō, S. Aoyama, S. Mukai and K. Ikeda, Nucl. Phys. **A588** (1995), 29c.
10) S. Aoyama, K. Katō and K. Ikeda, Phys. Rev. **C55** (1997), 2379.
11) M. Homma, T. Myo, K. Katō, Prog. Theor. Phys. **97** (1997), 561.
12) T. Myo and K. Katō, Prog. Theor. Phys. **98** (1997), 1275.
13) T. Berggren, Nucl. Phys. **A109** (1968), 265.
14) W. J. Romo, Nucl. Phys. **A116** (1968), 617.
15) T. Berggren and P. Lind, Phys. Rev. **C47** (1992), 768.
16) T. Vertse, P. Curutchet and R. J. Liotta, Phys. Rev. **C42** (1990), 2605.
17) T. Vertse, R. J. Liotta and E. Maglione, Nucl. Phys. **A584** (1994), 13.
18) T. Nakamura et al., Phys. Lett. **B331** (1994), 296.
19) K. Ieki et al., Phys. Rev. Lett. **70** (1993), 730.
D. Sackett et al., Phys. Rev. **C48** (1993), 118.
20) S. Shimoura, T. Nakamura, M. Ishihara, N. Inabe, T. Kobayashi, T. Kubo, R. H. Siemssen, I. Tanihata, Y. Watanabe, Phys. Lett. **B348** (1995), 29.
21) B. Gyarmati, A. T. Kruppa and K. F. Pal, Phys. Rev. **A41** (1990), 3469.
22) D. J. Millener, J. W. Olness, E. K. Warburton and S. S. Hanna, Phys. Rev. **C28** (1983), 497.
23) I. Tanihata, T. Kobayashi, O. Yamakawa, S. Shimoura, K. Ekuni, K. Sugimoto, N .Takahashi, T. Shimoda and H. Sato, Phys. Lett. **B206** (1988), 592.
24) T. Nakamura et al., Phys. Lett. **B394** (1997), 11.
25) T. Otsuka, M. Ishihara, N. Fukunishi, T. Nakamura and M. Yokoyama, Phys. Rev. **C49** (1994), R2289.
26) H. Sagawa, N. Van. Giai, N. Takigawa, M. Ishihara, K. Yazaki, Z. Phys. **A351** (1995), 385.
27) H. Sagawa, B. A. Brown and H. Esbensen, Phys. Lett. **B309** (1993), 1.
28) T. Otsuka, N. Fukunishi and H. Sagawa, Phys. Rev. Lett. **70** (1993), 1385.
29) F. M. Nunes, I. J. Thompson and R. C. Johnson, Nucl. Phys. **A596** (1996), 171.

30) P. Descouvemont, Nucl. Phys. **A615** (1997), 261.
31) F. Ajzenberg-selove, Nucl. Phys. **A506** (1989), 1.